Control of silver clustering for broadband Er^{3+} luminescence sensitization in Er and Ag co-implanted silica

Enrico Trave[a,*], Michele Back[a], Elti Cattaruzza[a], Francesco Gonella[a], Francesco Enrichi[a,b,c], Tiziana Cesca[d], Boris Kalinic[d], Carlo Scian[d], Valentina Bello[d], Chiara Maurizio[d], Giovanni Mattei[d]

[a] *Department of Molecular Sciences and Nanosystems, Ca' Foscari University of Venice, via Torino 155, 30172 Mestre, Venezia, Italy*

[b] *Division of Materials Science, Department of Engineering Sciences and Mathematics, Luleå University of Technology, 971 87 Luleå, Sweden*

[c] *Museo Storico della Fisica e Centro Studi e Ricerche Enrico Fermi, piazza del Viminale 1, 00184 Roma, Italy*

[d] *University of Padova, Physics and Astronomy Department, NanoStructures Group, via Marzolo 8, 35131 Padova, Italy*

ABSTRACT

In this work, the optical properties of Er and Ag co-implanted silica slabs were investigated in order to shed light on the observed improvement of the rare-earth emission properties through a sensitization process activated by Ag implantation. A full ion implantation approach was adopted since it represents an effective way to create a thin doped layer, where luminescent Er ions can interact with Ag-related sensitizing species. The results evi- denced that the sensitization process is effectively promoted in presence of Ag ultra-small structures, like few- atom aggregates or multimers, which can be already formed at the early stages of the metal clustering process. On the other hand, the precipitation of large, plasmonic clusters, occurring at high temperature post-Ag im- plantation annealing, produces a decrease of the fluorescence enhancement effect. Furthermore, it is suggested that the overall sensitization mechanism originates from an Ag-Er energy transfer that determines the possibility of a broadband photostimulation of the rare-earth ions, even by pumping in non-resonant excitation condition. Thanks to these features, the investigated Er and Ag co-implanted system can be considered for the realization of high-performing optical amplifiers in waveguide.

1. Introduction

The field of optical communications continuously requires the development of new materials for the transmission and the amplification of light signals. In this context, insulating matrices doped with rare- earth species have represented an active research field during the last decades [1–8]. Particularly, the superior chemical resistance and the compatibility to optical fiber technology make silica-based matrices one of the elective hosts for the realization of Er-based devices, since the ion can be naturally incorporated in an optically active site. Furthermore, silica glass can accommodate a wide variety of doping elements, whose structural and optical properties can be controlled and even tuned by suitable post-doping treatments. Depending on the functionality re- quired for a specific device, a crucial aspect is the possibility to improve the optical response of the rare-earth, being this species intrinsically characterized by small excitation cross-section values. With the aim at realizing Er-based waveguide systems with en- hanced optical performances, several synthesis techniques were ex- plored [3,9–12] to achieve a real improvement in terms of rare-earth distribution homogeneity, optimized doped layer geometry, limited structural defectivity. Furthermore, to enhance the Er luminescence, it is well established that the incorporation in the host of suitable co- doping species can lead to an overall intensity increase of the rare-earth emission features, including those falling within the telecommunication wavelength window (usually around 1.5 μm). As concerns the use of metallic species as rare-earth luminescence sensitizers, in the 80's a few papers reported about the possibility to increase of Eu^{3+} ion emissions in calcium boron oxyfluoride [13] and sol-gel derived silica glasses [14] after the incorporation of Ag pre- cursor and following precipitation of metallic nanoparticles (NPs). In the latter case, the authors proposed that the increased fluorescence stemmed from local-field enhancement around Eu ions owing to surface plasmon resonance (SPR) features occurring in the Ag NPs. At the turn of 2000's, it was demonstrated that for Eu [15,16] and Er [17,18] the presence of a silver surface near the region doped with optically active ions can relax the momentum mismatch between photon and the pro- pagating surface

plasmon waves. This process thus contributes to the far-field fluorescence of the rare-earth emitter, effectively increasing its radiative emission rate. The emission enhancement is attributed to near-field coupling of Er^{3+} to Ag surface plasmon polaritons, that subsequently re-radiate at well-defined resonance conditions. In the following years, the advent of plasmonics has determined a new para- digm for the realization of nanoscale devices operated at the optical and telecom wavelengths, thanks to novel functionalization in terms of light generation, manipulation and guiding, including the possibility to im- prove the emission properties of luminescent materials.

In addition to this research line, involving Plasmon-enhanced lu- minescence phenomena driven by metal NPs, it must be considered the pioneering work by Strohhöfer and Polman [19], that dealt with the luminescence sensitization effect occurring in Er-implanted borosilicate glasses after Ag ion-exchange procedure. Supported by following stu- dies, it was evidenced that the presence of ultra-small, non-plasmonic Ag clusters promotes the activation of a non-resonant energy transfer process to the Er^{3+} ions, then determining the broadening and the enhancement of the rare-earth absorption spectrum, with consequent improvement of the luminescence activity [20–24]. Furthermore, these sensitizing Ag-related species, whose formation characterizes the early stage of the overall clustering process, exhibit peculiar luminescence activity characterized by spectral band across the UV–visible range [25–27]. Later, several studies focused the occurrence of luminescence en- hancement effects driven by different metal sensitizing agents, like Au [28–32], Cu [33–35], Sn [36], Bi [37], for Er ions and, more in general, for other rare-earth species [38–42]. It is worth pointing out that the photophysical mechanism at the basis of the interaction between rare- earth and Ag (or metal) sensitizing species strongly resembles the well- known Er broadband sensitization process promoted by the coupling with Si nanocluster-based energy transfer mediators [43–47].

In this work, we investigated the optical properties of Er and Ag co-doped silica thin films, focusing on the occurrence of a rare-earth lu- minescence improvement through the coupling with metal sensitizers. The samples were prepared by a full ion implantation route, since this technique represents an efficient way to generate a homogeneous, step- like active layer with controlled dopant concentration, even beyond the solubility limit allowed by the specific host. Then, metal clustering process was promoted and carefully controlled by following post-im- plantation heating treatment, for an effective size tuning of the pre- cipitated nanostructures. Spectroscopic and time-resolved photo- luminescence studies were carried out with the aim at determining the best conditions for material synthesis and processing, in order to maximize the Ag-driven Er sensitization process and thus the yield of the rare-earth luminescence emission at 1.54 μm.

2. Experimental

2.1. Sample preparation

Sequential ion implantation procedures were carried out on silica substrates (Herasil 102 by Haereus; slide area of 7.5×2.5 cm^2) at room temperature for preparing a series of Er and Ag co-doped samples. To obtain step-like concentration profile and to extend the doped region, a sequence of three consecutive implantations at specific energies were used for both the doping elements. Fluence and implant energy values were chosen for optimizing the overlap of the respective concentration profiles. Post-implantation thermal treatments were performed with a proper choice of heating conditions, such as temperature, atmosphere and duration, in order to achieve the full recovery the implantation induced damage and, consequently, to promote optical activation of Er^{3+} ions as well as the control of metal diffusion and aggregation processes. First, Er ions were incorporated into pristine silica substrates by an implantation sequence at three different energies (50, 100, 190 keV), 2 with current densities of about 0.05μA/cm and a total dose of 6.8×10^{14} Er^{+}/cm^2, as estimated by Rutherford Backscattering Spectrometry (RBS); the Er-doped layer thickness resulted of about 100 nm, centered at a depth of about 70 nm. The Er-doped slides were then heated at 900 °C, for 1 h, in N_2 atmosphere to activate the char- acteristic Er luminescence emissions. Except for one of the Er-doped samples, labelled as Er reference and used as reference for the optical measurements, the others underwent a further triple implantation procedure with Ag ions at three different energies (45, 90, 190 keV) in order to have a homogeneous Ag con- centration profile over the Er-doped layer. The ion beam current den- sity was set at about 0.5 μA/cm^2 for all the implantations, whereas the total dose resulted of 6.1×10^{15} Ag^{+}/cm^2 (from

RBS measurement) over a doped region of about 100 nm thickness, determining an overall limited level of metal concentration, and then preventing a massive cluster precipitation. In this way, the evolution of the Ag aggregation was controlled by suitable post-implantation thermal treatments. Moreover, it is worth considering that small implantation current density values were used in these experiments to prevent possible metal aggregation promoted by substrate heating and increase in the diffusion mobility of incorporated Ag ions [48]. Post-implantation thermal treatments were carried out in N_2 atmosphere, for 1h, in the temperature range from 400 to 900 °C. Table 1 reports the list of the in- vestigated samples, including the respective label referred to the post- Ag implantation annealing temperature, and the RBS estimation of the Er and Ag dose.

2.2. Optical and structural characterization

Photoluminescence (PL) investigation was carried out by using an experimental set-up dedicated to the study of the Er ion luminescence properties. Sample excitation was obtained by means of a cw Ar laser, whose emission lines at 488 and 476.5 nm allow for Er ion photo-sti- mulation in resonance and out-of-resonance conditions, respectively: in the former case, the excitation wavelength matches the transition from the Er^{3+} $^4I_{15/2}$ ground state to the $^4F_{7/2}$ excited level, whereas in the latter the pumping radiation cannot be directly absorbed by the rare- earth ion. The laser beam was of about 1 mm in diameter and it was modulated by a mechanical chopper. PL emission was detected using a single-grating monochromator equipped with a nitrogen-cooled pho- tomultiplier tube operating in the 1000–1650 nm spectral range, then the signal was acquired with a lock-in amplifier, using the chopper frequency as reference. PL excitation (PLE) measurements were performed by pumping the samples with a 150 W Xe lamp coupled to a monochromator, operated in the 250–800 nm range. PL dynamics investigation was carried out by collecting the time decay curves with an oscilloscope (overall time resolution of about 5 μs). Optical absorbance spectra in the UV–Vis region (250–900nm) were recorded at room temperature using a Jasco V670 spectro- photometer. Microstructural characterization was performed by transmission electron microscopy (TEM) with a FEI Tecnai Field-emission Gun (FEG) (S)TEM F-20 Super Twin, operating at 200 keV, equipped with an EDAX energy-dispersive X-ray spectrometer (EDS). Rutherford backscattering spectrometry (RBS) measurements were performed at INFN National Laboratories of Legnaro, Italy (LNL) with a 2.2 MeV $^4He+$ beam, at a scattering angle of 160°. Er and Ag contents (expressed as dose in atoms/cm^2) were calculated by simulation of the RBS spectra with the RUMP code [49].

3. Results and discussion

3.1. Enhancement of 1.54 μm Er^{3+} emission

The occurrence of a photosensitization process after the incorpora- tion of Ag ions in Er implanted silica has been evidenced by a lumi- nescence study of the rare-earth emission around 1540 nm, both in resonant and non-resonant pumping conditions. To this aim, we used the 488 and the 476.5 nm emission lines of an Ar laser operated at 6.5 mW and mechanically chopped at 9 Hz. Fig. 1 presents a comparison between the PL spectra in the 1450–1650 nm range of the Er reference sample and the co-implanted sample after 600 °C treatment, labelled as Er+Ag 600 °C, which results the best performing one in terms of the improvement of the Er ion emission. To better appreciate the parallel, the intensity of the spectra related to the co-implanted sample was divided by a factor of 10. By exciting both samples at a wavelength of 488 nm, which is resonant with the Er^{3+} $^4I_{15/2} \rightarrow {}^4F_{7/2}$ ground-to-excited state transition, a more intense PL signal was measured for the Er+Ag 600 °C sample than the reference one, showing an enhancement factor of about 25 for the emission at 1.54 μm. Furthermore, it is worth noticing that the metal ion implantation did not affect the structural environment surrounding the Er^{3+} ions, since the shape of the PL peak remains unchanged after Ag co-doping, with the same bandwidth of 27 nm. Nevertheless, another significant finding must be highlighted in Fig. 1: for the co-implanted sample, the 1.54 μm PL emission occurs even under laser excitation at 476.5nm, a wavelength not directly absorbed by the Er^{3+} ions, and the intensity of the signal is comparable to the one obtained by resonant pumping. This is a clear indication of the effectiveness of the coupling between the optically active Er ions and the Ag-related centers responsible for the PL enhancement. More- over, it can be suggested that Er^{3+} ions are mainly excited via an Ag- mediated, indirect path, while the direct Er^{3+} light

absorption provides a negligible contribution to the measured 1.54 μm emission signal. To figure out the impact of the metal clustering process and to find the best conditions for an efficient Er^{3+} sensitization, the influence of the thermal treatment conditions on the Er luminescence properties was studied, by performing isochronal (1 h) post-implantation annealing in N_2 atmosphere, in the 400–900 °C temperature range, after silver implantation. It is worth remarking that matrix recovery by thermal treatment is of paramount importance to remove the implantation-in- duced defective centers, that can optically interact with the excited Er ion and then open an effective non-radiative relaxation channel, with consequent luminescence emission quenching. Fig. 2 reports the 1.54 μm PL emission of different co-doped samples as a function of the annealing temperature in both resonance and out- of-resonance pumping conditions, normalized to the PL signal of the Er reference sample excited at 488 nm. The first evidence is that, already after Ag implantation, Er PL enhancement takes place: by both resonant and non-resonant Ar laser excitation, the PL signal of Er and Ag as- implanted sample is twice as intense as the Er reference sample. Upon thermal treatment, a progressive enhancement is obtained by in- creasing the temperature up to 600 °C. Above this threshold limit, the PL signal significantly drops off, with the 900 °C annealed sample ex- hibiting an emission intensity comparable to the Er reference one, with no signal by pumping in out-of-resonance condition. As concerns the PL signal increase in the low annealing temperature regime, the heat-induced formation of many energy transfer centers may therefore promote the increase of the rare-earth emission at 1.54 μm. On the other hand, one must also consider the direct impact of the annealing step on the Er^{3+} luminescence dynamics. In fact, it is well known that the thermal treatment induces the bleaching of the matrix defects generated by implantation, increasing the emission lifetime and so the PL quantum efficiency. This can be appreciated by observing the evolution of the time decay curves for 1.54 μm Er^{3+} emission reported in Fig. 3, that attests a progressive lifetime rise with the annealing temperature.

Concerning the shape of the reported curves, it is worth noticing that after post-Ag implantation annealing in the low temperature re- gime (up to about 400–500 °C), the PL signal decay follows an evident non-exponential trend, which could be owed to a lack in homogeneity of the local environment for the optically active Er ions. In fact, a fraction of these should be located in highly defective sites character- ized by ion relaxation dynamics heavily affected by non-radiative processes, which seem to be almost completely annealed out by a 600 °C treatment. At this temperature, the time decay curve exhibits a single-exponential trend, with a lifetime estimated of 11.8 ms. In this scenario, a further enhancement of the Er luminescence for treatment temperature over 600 °C should be expected. The lifetime increase is actually observed in this temperature regime, reaching a value of 12.6 ms for the 900 °C annealed sample, which is comparable to the estimate of 12.9ms obtained for the Er reference one. Nevertheless, as stated above, an evident decrease of the PL emission occurs starting from the Er+Ag 700°C sample, with an out-of-re- sonance signal clearly weaker than under 488 nm pumping. This could be related to the fact that the mechanism bringing to the rare-earth enhancement becomes less effective, due to the dissolution of the Ag- related sensitizing centers, being the Er ions mainly excited by the di- rect absorption path involving the transition from the ground state to the $^4F_{7/2}$ excited level. To give account for this observation, we must consider that the Ag diffusion mobility is enhanced upon heating, thus leading to an efficient particle nucleation and growth processes with the formation of nano- particles larger as the temperature increases. This could determine a decreasing number of sensitizers per unit volume. In addition, the heating treatment can also promote Ag thermal diffusion, with the modification of the metal concentration profile and possible decoupling between Ag-related sensitizers and Er ions. Furthermore, the trend shown by the RBS dose estimates reported in Table 1 suggests that also Ag out-diffusion process can take place, leading to a progressive de- crease of the metal content in the glass as the temperature rises. All these phenomena can determine the complete switching-off of the sensitization effect for both samples annealed at 800 °C and 900 °C, as shown in Fig. 2.

3.2. Ag clustering process

Since the Er luminescence behaviour in the co-doped system is strictly connected to the metal aggregation state, we investigated the optical absorption properties exhibited by the synthesized glasses in order to shed light on the evolution of the metal clustering process driven by the thermal annealing procedure. In fact, it is well known that metal clusters in dielectric hosts exhibit striking optical properties, and in particular the ones deriving from the activation of the so-called surface plasmon resonance (SPR) phenomenon [50–53]. As shown in Fig. 4, starting from an annealing temperature of 500 °C the optical profile of the co-doped sample

is characterized by the enhancement of an absorption band peaked around 400–420 nm, which is the peculiar fingerprint of SPR processes in small metallic Ag clusters in glass. Concerning the intensity of the SPR band, its contribution to the overall optical absorbance spectrum in a composite system is strongly damped for very small clusters (diameter ≤ 1 nm) [54–57]. Therefore, by observing the trend of the spectra in Fig. 4 it can be argued that Ag implantation in our experimental conditions induces the precipitation of clusters of few atoms rather than nanoparticles big enough to support the plasmon resonance. As stated above, after suitable heating the silver SPR band is peaked at the UV–visible edge and undergoes a progressive narrowing as the temperature increases. This effect is due to the pre- cipitation of larger and larger clusters as the temperature rises, since Mie theory predicts a decrease of the peak width as the cluster size increases at least up to a few tens of nanometers [58]. Moreover, one should expect the observed width narrowing to be accompanied by a SPR band enhancement; instead, the plasmonic feature is significantly weakened for the Er+Ag 800 °C and Er+Ag 900 °C samples. This fact is likely due to the occurrence of Ag out-diffusion process, evidenced by the RBS analysis, which implies a progressive decrease of the metal content in the matrix and a significant reduction of the cluster density. However, in Fig. 4 we also observe a surprising behaviour related to the occurrence of a blue-shift of the SPR peak position with increasing temperature, and consequently as the cluster size increases, going from 420 nm for the Er+Ag 600 °C sample to 400 nm for the Er+Ag 900 °C one. To explain this evidence, it can be argued that at lower annealing temperatures the host is permeated by a high density of small clusters, resulting in a considerably reduced interparticle distance. In this way, multipole interactions between neighbouring particles could determine a SPR peak red-shift in comparison to the Mie's case [58,59]. Another way to restate this hypothesis is in the frame of the effective medium theory: due to the out-diffusion process, the silver content decreases as the annealing temperature increases, and then the average dielectric function of the composite tends asymptotically to that of the matrix without silver, producing an evident blue-shift of the SPR peak position. Furthermore, the occurrence of intrinsic size effects for the Ag na- noclusters must be also taken into account [54,60]. Shift of the plasmon resonance at larger wavelengths for ultra-small clusters could be due to the occurrence of the spill-out effect, where valence electrons come out from the metal cluster surface leading to an increased polarizability of the system. Therefore this effect is expected to lose its effectiveness as the cluster size increases, then determining the observed SPR peak blue- shift as the temperature rises.

Further information about the metal clustering process was achieved through the structural characterization resulting from the TEM analysis. Our investigation focused the Er+Ag 600 °C and Er+Ag 900°C samples, as representative of a situation of maximized and ceased Er sensitization effect, respectively. In Fig. 5, BFTEM cross section micrographs of Er and Ag co-im- planted samples annealed at 600 °C (a) and 900 °C (b) show spherical Ag nanoclusters, whose average size is an increasing function of the annealing temperature. The Er+Ag 600°C sample exhibits a high density of small clusters characterized by an in-depth distribution evi- dencing the early-stage of the silver out-diffusion process. Indeed, the region where Ag clusters can be observed extends from the sample surface towards the interior of the glass slide, while the centroid of the metal concentration is slightly shifted towards the sample surface with respect to the Er-doped layer. In this regard, the observation of such metal depletion phenomenon well agrees with the progressive decrease of the Ag retained dose estimated by RBS (see Table 1). Moreover, in Fig. 5(a) it is worth noticing the presence of Ag na- noparticles just outside the silica surface, exhibiting spherical shape and size comparable with those located inside the host matrix. On the other hand, the sample annealed at 900 °C exhibits a different mor- phology. In the region below the surface, the cross section view in Fig. 5(b) shows the presence of a quite homogeneous distribution of Ag clusters more dispersed and larger in size than in the Er+Ag 600 °C sample, even though small aggregates are clearly observable. Further- more, for the Er+Ag 900 °C sample one can notice an almost complete absence of particles at the surface, with a sort of cluster depletion just beneath the surface. This fact is likely related to metal evaporation phenomena, since at high annealing temperatures the particles on the surface tend to undergo melting and evaporation processes. This can be explained considering the well-known lowering of the melting tem- perature of the clusters with respect to the bulk value (961 °C for silver) due to the thermodynamic size effect when the cluster radius decreases [61,62].

HRTEM analysis allowed to explore the structure of the Ag nano- particles at atomic level. In the high-resolution image of Fig. 5(c) and (d), corresponding to the sample heated at 600 °C and 900 °C, respec- tively, metal aggregates with a diameter of about 4–5 nm exhibit a well- defined crystalline structure, characterized by the typical (111) lattice plane fringes of the metallic Ag fcc structure. A statistical analysis of the nanocrystal size distribution was per- formed to evaluate the mean diameter $< D >$; TEM histograms

and fit results are reported in Fig. 5(e) and (f). Both the cluster mean diameter and the standard deviation σ increase with the annealing temperature. In fact, the mean diameter increases from 2.2 nm after 600 °C annealing to 3.7 nm at 900 °C, with σ values of 0.8 and 1.9 nm, respectively. Al- though the size distribution histograms are characterized by the pre- sence of clusters with diameter up to about 5 nm for the Er+Ag 600 °C sample and to about 10nm for the Er+Ag 900°C one, it is worth stressing the presence of a fraction of Ag clusters with ultra small di- mension (≤ 1 nm) in both histograms. The observed metal clustering process can be explained in the fra- mework of the particle nucleation and growth theory [63]. As a general scheme, at first the clustering process involves the formation of metal embryos by both homogeneous and heterogeneous nucleation processes [64], already active during the implantation process, with the sub- sequent particle growth when the radius value exceeds the critical one. During the annealing treatment, cluster scaling-up occurs by direct solute depletion of the surrounding matrix, without interaction between the growing particles, and the overall process takes place in the so- called diffusion-limited aggregation regime. When the degree of su- persaturation becomes extremely small, a new phase in the precipita- tion process takes place, where large particles continue to grow while smaller ones dissolve. This stage is known as coarsening [65,66], also referred as Ostwald ripening if the whole process occurs under mass conservation conditions.

3.3. Er^{3+} sensitization mechanism

To get deeper inside the sensitization mechanism involving light absorption by Ag-related centers and the activation of Er ion emission at 1.54 μm, PL excitation measurements were performed by using of a broad spectrum Xe lamp coupled to a monochromator for the wave- length tuning. Spectral analysis considers the emission intensity at a fixed detection wavelength (1.54 μm in the present case) as a function of the excitation wavelength. The PLE spectrum is strongly dependent on the variation of the absorption cross- section with the pumping wa- velength. In fact, at low excitation intensities the PL intensity can be expressed as a function of the excitation wavelength λ_{exc} as

$$I(\lambda) \propto Nact\ \sigma(\lambda exc)\ \varphi(\lambda exc)\ P(\lambda exc)\ \eta PL$$

where N_{act} is the total number of optically active Er ions, $\sigma(\lambda_{exc})$ and $\varphi\ (\lambda_{exc})$ are the Er^{3+} absorption cross-section and the photon flux at specific λ_{exc}, respectively, $P_{rel}(\lambda_{exc})$ accounts for the probability of ex- citation relaxation to the emitting energy level (in this case the $^4I_{13/2}$ energy level) and η is the quantum efficiency of the spontaneous emission from that level to the $^4I_{15/2}$ ground state. Fig. 6 reports the comparison between the PLE spectrum of the signal recorded at 1.54 μm for the Er+Ag 600 °C (red line) and the Er reference (gray line) samples. While the Er reference spectrum exhibits a series of peaks due to the different transitions occurring from the ground state to the higher-lying energy levels (see in the inset of Fig. 6), in the case of the co-implanted sample the rare-earth ions can be sti- mulated over a continuous range of excitation wavelengths, with a threshold at about 600 nm and an upward profile going towards the UV region. Floating on this broad excitation band, one can observe a couple of weak features falling in wavelength ranges resonant with the direct transition from the ground state to the $^4G_{11/2}$ (379 nm) and the $^2H_{11/2}$ (520 nm) manifolds, respectively, which are among the most sensitive absorption lines exhibited by Er ions in silica (for σ of about 10^{-19} cm^2 in both cases). However, the contribution deriving from direct rare- earth ion excitation seems negligible, and it can be claimed that the Er PL enhancement originates from the activation of an alternative ex- citation path driven by Ag-related optically active species, character- ized by a wide light absorption spectrum.

The possibility to pump the Er ions using a broadband excitation source, with a manifest increase of the signal at 1.54 μm, is extremely appealing from a technological point of view. In fact, a significant im- provement on the performances of optoelectronic devices, such as op- tical amplifiers, can be achieved since in this system cheap, broadband pumping lamp can efficiently replace the 980 nm or 1480 nm light sources commonly used in commercial Er-doped devices. Significant considerations about the Er enhancement mechanism, then regarding the nature of the Ag-related sensitizers, can be obtained from the comparison provided in Fig. 6, between the PLE spectrum at 1.54 μm and the optical absorbance measure for the Er+Ag 600 °C sample. What firstly emerges is that the spectral shape of the PLE measurement does not match the

observed plasmonic band character- izing the overall absorption profile in the UV–visible range. This first impressive evidence rules out the influence of a local-field enhancement due to SPR on the mechanism responsible for the Er luminescence in- crease, as instead observed in the case of the Eu^{3+} PL improvement through the interaction with Ag nanoparticles [13,14]. Furthermore, the absorption signal covers almost entirely the visible range up to the near-IR edge, while, as emerging from PLE measure- ments, it seems that the Er^{3+} ions are not significantly excited at wa- velengths higher than 600 nm. The silver plasmonic band is therefore supposed to hide the absorption feature that determines the initial step in the indirect path for excitation of the rare-earth ions. These ob- servations allow to conclude that the PL enhancement is due to a photosensitization mechanism involving light absorption from Ag-re- lated sensitizing centers and the subsequent resonant energy transfer to the Er ions, whereas Ag nanoparticles do not contribute to this process by SPR local-field enhancement. As suggested by Strohhöfer and Polman [19], and considering that in the early stage of the clustering process a certain fraction of silver is still in form of ultra-small ag- gregates (with size ≤ 1 nm), such as clusters of few atoms and multi- mers, this kind of Ag structures are therefore supposed to play a major role in the Er^{3+} sensitization process, being photoactivated through light absorption in a broad energy range. It is worth noticing that several works can be found in literature dealing with the luminescence properties in the UV–visible range of Ag in form of ions, pairs, multimers, small clusters embedded in glassy hosts [67–73]. Therefore, it is suggested that the possible activation of an Ag-driven energy transfer process to other luminescent species, like Er^{3+} or other rare-earth ions, can be determined by the spectral overlap between the respective emission and excitation spectra.

4. Conclusions

We investigated the broadband enhancement of the 1.54 μm emis- sion in Er and Ag co-doped silica slabs, realized by a full ion im- plantation approach. The increase of Er^{3+} PL emission at 1.54 μm is due to a photosensitization mechanism originating from light absorption by few-atom Ag clusters or multimeric structures in a wide wavelength range, and subsequent energy transfer towards the rare-earth ions, while an improvement induced by a local field enhancement due to surface plasmon resonance at the Ag nanoparticles can be excluded. A noteworthy observation is that the Er sensitization process is al- ready active after metal incorporation, indicating that ultra-small Ag aggregates can efficiently mediate the energy transfer process to the Er ions. Following the evolution of both structural and optical properties of the co-implanted glasses, it was observed that the luminescence re- sponse of the system can be optimized by a proper choice of the post- implantation annealing conditions, balancing between the matrix re- covery from implantation-induced defects, and the control of the Ag clustering evolution. In fact, on one hand the rise of the annealing temperature is associated to an enhanced optical quality of the glassy samples, corresponding to an increase of 1.54 μm Er emission lifetime. On the other hand, the use of high treatment temperatures (i.e., 800–900 °C) involves the extinction of the Er^{3+} PL sensitization effect, likely due to both the precipitation of large Ag nanoparticles with consequent decrease of the number of the aggregates acting as energy transfer mediators, and the strengthening of the Ag out-diffusion pro- cess, leading to an overall reduction of the metal content. Therefore, the full improvement of the rare-earth luminescence response was achieved by using moderate annealing temperatures. In fact, the most intense emission at 1.54 μm was observed for the co-doped sample heated at 600 °C, giving rise to an enhancement factor of about 25 compared to the Er reference signal. In conclusion, this work demonstrated that ion implantation in glass is a suitable route for obtaining Er-doped thin films, where the rare- earth luminescence response is enhanced by a photosensitization pro- cess determined by an energy transfer mechanism mediated by few- atom Ag aggregates or multimeric structures. In view of optoelectronic applications, like the realization of light amplifiers in waveguide, it is worth considering the evident increase of the PL signal at 1.54 μm, together with the possibility of a broadband pumping of the rare-earth ions over a wavelength range extended to the UV–visible range.

Acknowledgments

The NanoStructures Group gratefully acknowledges the Italy- Mexico Project of Major Importance (MX14MO09) of the Italian Ministry of Foreigner Affairs and International Cooperation (MAECI). Francesco Enrichi gratefully acknowledges VINNOVA for support, under the Vinnmer Marie Curie Incoming - Mobility for Growth Programme (project “Nano2solar” Ref. No. 2016-02011) and the PLESC

Project between South Africa and Italy (contributo del Ministero degli Affari Esteri e della Cooperazione Internazionale, Direzione Generale per la Promozione del Sistema Paese).

References

[1] W.J. Miniscalco, Erbium-doped glasses for fiber amplifiers at 1500 nm, J. Lightw. Technol. 9 (1991) 234–250.

[2] E. Desurvire, The golden-age of optical-fiber amplifiers, Phys. Today 47 (1994) 20–27.

[3] A. Polman, Erbium implanted thin film photonic materials, J. Appl. Phys. 82 (1997) 1–39.

[4] J.D.B. Bradley, M. Pollnau, Erbium-doped integrated waveguide amplifiers and lasers, Laser Photon. Rev. 5 (2011) 368–403.

[5] K. Binnemans, Lanthanide-based luminescent hybrid materials, Chem. Rev. 109 (2009) 4283–4374.

[6] K.S. Abedin, T.F. Taunay, M. Fishteyn, M.F. Yan, B. Zhu, J.M. Fini, E.M. Monberg, F.V. Dimarcello, P.W. Wisk, Amplification and noise properties of an erbium-doped multicore fiber amplifier, Opt. Express 19 (2011) 16715–16721.

[7] G. Bellocchi, G. Franzò, F. Iacona, S. Boninelli, M. Miritello, T. Cesca, F. Priolo, Eu^{3+} reduction and efficient light emission in Eu_2O_3 films deposited on Si sub- strates, Opt. Express 21 (2012) 5501–5507.

[8] G. Bellocchi, F. Iacona, M. Miritello, T. Cesca, G. Franzò, SiOC thin films: an effi- cient light source and an ideal host matrix for Eu^{2+} ions, Opt. Express 21 (2013) 20280–20290.

[9] E.M. Yeatman, M.M. Ahmad, O. McCarthy, A. Martucci, M. Guglielmi, Sol-gel fabrication of rare-earth doped photonic components, J. Sol-Gel Sci. Technol. 19 (2000) 231–236.

[10] E. Cattaruzza, G. Battaglin, F. Visentin, E. Trave, Er-doped SiO_2 films by rf mag- netron Co-sputtering, J. Non-Cryst. Solids 355 (2009) 1128–1131.

[11] E. Cattaruzza, G. Battaglin, F. Gonella, C. Maurizio, S. Ali, E. Trave, Doping of silicate glasses with erbium by a field-assisted solid-state ion exchange technique, J. Phys. D Appl. Phys. 42 (2009) 045301.

[12] J. Rönn, L. Karvonen, C. Kauppinen, A.P. Perros, N. Peyghambarian, H. Lipsanen, A. Säynätjoki, Z. Sun, Atomic layer engineering of Er-ion distribution in highly doped Er:Al_2O_3 for photoluminescence enhancement, ACS Photonics 3 (2016) 2040–2048.

[13] O.L. Malta, P.A. Santa-Cruz, G.F. de Sá, F. Auzel, Fluorescence enhancement in- duced by the presence of small silver particles in Eu^{3+}-doped materials, J. Lumin. 33 (1985) 261–272.

[14] T. Hayakawa, S.T. Selvan, M. Nogami, Field enhancement effect of small Ag and Sub-nanometric metallic Au clusters as efficient Er^{3+} sensitizers in silica, Appl. Phys. Lett. 89 (2006) 151121.

[15] R.M. Amos, W.L. Barnes, Modification of spontaneous emission lifetimes in the presence of corrugated metallic surfaces, Phys. Rev. B 59 (1999) 7708–7714.

[16] P. Andrew, W.L. Barnes, Molecular fluorescence above metallic gratings, Phys. Rev. B 64 (2001) 125405.

[17] J. Kalkman, C. Strohhöfer, B. Gralak, A. Polman, Surface plasmon polariton modified emission of erbium in a metallodielectric grating, Appl. Phys. Lett. 83 (2003) 30–32.

[18] J. Kalkman, L. Kuipers, A. Polman, H. Gersen, Coupling of Er ions to surface plasmons on Ag, Appl. Phys. Lett. 86 (2005) 041113.

[19] C. Strohhöfer, A. Polman, Silver as a sensitizer for erbium, Appl. Phys. Lett. 81 (2002) 1414–1416.

[20] P. Mazzoldi, S. Padovani, F. Enrichi, G. Mattei, E. Trave, M. Guglielmi, A. Martucci, G. Battaglin, E. Cattaruzza, F. Gonella, C. Maurizio, Sensitizing effects in Ag-Er co-doped glasses for optical amplification, SPIE Proc. 5451 (2004) 311–326.

[21] A. Martucci, M. de Nuntis, A. Ribaudo, M. Guglielmi, S. Padovani, F. Enrichi, G. Mattei, P. Mazzoldi, C. Sada, E. Trave, G. Battaglin, F. Gonella, E. Borsella, M. Falconieri, M. Patrini, J. Fick, Silver sensitized erbium doped ion exchanged sol-gel waveguides, Appl. Phys. A: Mater. Sci. Process. 80 (2005) 557–563.

[22] M. Mattarelli, M. Montagna, K. Vishnubhatla, A. Chiasera, M. Ferrari, G.C. Righini, Mechanisms of Ag to Er energy transfer in silicate glasses: a photoluminescence study, Phys. Rev. B 75 (2007) 125102.

[23] M. Eichelbaum, K. Rademann, Plasmonic enhancement or energy transfer? On the luminescence of gold-, silver-, and lanthanide-doped silicate glasses and its potential for light-emitting devices, Adv. Funct. Mater. 19 (2009) 2045–2052.

[24] M. Tiwary, N.K. Singh, S. Annapoorni, D.C. Agarwal, D.K. Avasthi, Y.K. Mishra, P. Mazzoldi, G. Mattei, C. Sada, E. Trave, G. Battaglin, Enhancement of photo- luminescence in Er-doped Ag-SiO_2 nanocomposite thin films: a post annealing study, Vacuum 85 (2011) 806–809.

[25] M. Mattarelli, M. Montagna, E. Moser, K.C. Vishnubhatla, C. Armellini, A. Chiasera, M. Ferrari, G. Speranza, M. Brenci, G.N. Conti, G.C. Righini, Silver to erbium energy transfer in phosphate glasses, J. Non-Cryst. Sol. 353 (2006) 498–501.

[26] M. Eichelbaum, K. Rademann, A. Hoell, D.M. Tatchev, W. Weigel, R. Stößer, G. Pacchioni, Photoluminescence of atomic gold and silver particles in soda-lime silicate glasses, Nanotechnology 19 (2008) 135701.

[27] E. Trave, F. Gonella, P. Calvelli, E. Cattaruzza, P. Canton, D. Cristofori, A. Quaranta, G. Pellegrini, Laser beam irradiation of silver doped silicate glasses, Nucl. Instrum. Methods Phys. Res. B 268 (2010) 3177–3182.

[28] E. Trave, G. Mattei, P. Mazzoldi, G. Pellegrini, C. Scian, C. Maurizio, G. Battaglin, Sub-nanometric metallic Au clusters as efficient Er^{3+} sensitizers in silica, Appl. Phys. Lett. 89 (2006) 151121.

[29] C. Maurizio, E. Trave, G. Perotto, V. Bello, D. Pasqualini, P. Mazzoldi, G. Battaglin, T. Cesca, C. Scian, G. Mattei, Enhancement of the Er^{3+} luminescence in Er-doped silica by few-atom metal aggregates, Phys. Rev. B: Condens. Matter Mater. Phys. 83 (2011) 195430.

[30] T. Cesca, B. Kalinic, C. Maurizio, C. Scian, G. Battaglin, P. Mazzoldi, G. Mattei, Near-infrared room temperature luminescence of few-atom Au aggregates in silica: a path for the energy-transfer to Er^{3+} ions, Nanoscale 6 (2014) 1716–1724.

[31] T. Cesca, B. Kalinic, C. Maurizio, C. Scian, G. Battaglin, P. Mazzoldi, G. Mattei, Interatomic coupling of Au molecular clusters and Er^{3+} ions in silica, ACS Photonics 2 (2015) 96–104.

[32] T. Cesca, B. Kalinic, C. Maurizio, N. Michieli, C. Scian, G. Mattei, Amplified sensi- tization of Er^{3+} luminescence in silica by Au_N quantum clusters upon annealing in a reducing atmosphere, RSC Adv. 6 (2016) 99376–99384.

[33] E. Cattaruzza, G. Battaglin, F. Visentin, E. Trave, G. Aquilanti, G. Mariotto, Enhanced photoluminescence at λ = 1.54 μm in Cu-doped Er:SiO_2 system, J. Phys. Chem. C 116 (2012) 21001–21011.

[34] E. Trave, E. Cattaruzza, P. Riello, Er and Cu codoped SiO_2 films obtained by sput- tering deposition: enhancement of the rare earth emission at 1.54 μm mediated by metal sensitizers, Opt. Mater. 35 (2013) 2018–2022.

[35] J.A. Jimenez, M. Sendova, Enhanced 1.53 μm emission of Er^{3+} ions in phosphate glass via energy transfer from Cu^{+} ions, J. Appl. Phys. 116 (2014) 033518.

[36] J.A. Jimenez, M. Sendova, B. Hosterman, Sn centers-mediated enhancement of 1.53 3+ μm emission of Er ions in phosphate glass, Mater. Lett. 131 (2014) 344–346.

[37] M. Back, E. Trave, R. Marin, N. Mazzucco, D. Cristofori, P. Riello, Energy transfer in Bi- and Er-codoped Y_2O_3 nanocrystals: an effective system for rare earth fluorescence enhancement, J. Phys. Chem. C 118 (2014) 30071–30078.

[38] J.A. Jimenez, M. Sendova, In situ isothermal monitoring of the enhancement and quenching of Sm^{3+} photoluminescence in Ag co-doped glass, Sol. State Commun. 152 (2012) 1786–1790.

[39] J.A. Jimenez, Twofold-coordinated tin centers as UV sensitizers of trivalent dysprosium ions, J. Non-Cryst. Solids 387 (2014) 124–127.

[40] R. Chattopadhyay, A. Haldar, M.C. Paul, S. Das, S.K. Bhadra, Quantum sized Ag nanocluster assisted fluorescence enhancement in Tm^{3+}-Yb^{3+} doped optical fiber beyond plasmonics, Appl. Phys. Lett. 107 (2015) 233107.

[41] J.A. Jimenez, Carbon-promoted in situ evolution of Cu nanoclusters influencing Eu^{3+} photoluminescence in glass: bidirectional energy transfer, J. Phys. Chem. C 120 (2016) 3557–3563.

[42] F. Enrichi, C. Armellini, G. Battaglin, F. Belluomo, S. Belmokhtar, A. Bouajaj, E. Cattaruzza, M. Ferrari, F. Gonella, A. Lukowiak, M. Mardegan, S. Polizzi, E. Pontoglio, G.C. Righini, C. Sada, E. Trave, L. Zur, Silver doping of silica-hafnia 3+ cells, Opt. Mater. 60 (2016) 264–269.

[43] M. Fuji, M. Yoshida, Y. Kanzawa, S. Hayashi, K. Yamamoto, 1.54 μm photo-luminescence of Er 3+ doped into SiO_2 films containing Si nanocrystals: evidence for energy transfer from Si nanocrystals to Er^{3+}, Appl. Phys. Lett. 71 (1997) 1198–1200.

[44] C.E. Chryssou, A.J. Kenyon, T.S. Iwayama, C.W. Pitt, D.E. Hole, Evidence of energy coupling between Si nanocrystals and Er^{3+} in ion-implanted silica thin films, Appl. Phys. Lett. 75 (1999) 2011–2013.

[45] P.G. Kik, M.L. Brongersma, A. Polman, A Strong exciton-erbium coupling in Si nanocrystal-doped SiO_2, Appl. Phys. Lett. 76 (2000) 2325–2327.

[46] F. Priolo, G. Franzò, D. Pacifici, V. Vinciguerra, F. Iacona, A. Irrera, Role of the energy transfer in the optical properties of undoped and Er-doped interacting Si nanocrystals, J. Appl. Phys. 89 (2001) 264–272.

[47] F. Enrichi, G. Mattei, C. Sada, E. Trave, D. Pacifici, G. Franzò, F. Priolo, F. Iacona, M. Prassas, M. Falconieri, E. Borsella, Evidence of energy transfer in an alumino- silicate glass codoped with Si nanoaggregates and Er^{3+} ions, J. Appl. Phys. 96 (2004) 3925–3932.

[48] A.L. Stepanov, V.N. Popok, Effect of the ion beam current density on the formation of implanted metal nanoparticles in a dielectric matrix, Tech. Phys. Lett. 29 (2003) 977–979.

[49] L.R. Doolittle, Algorithms for the rapid simulation of Rutherford backscattering spectra, Nucl. Inst. Methods B9 (1985) 344–351.

[50] G.C. Papavassiliou, Optical properties of small inorganic and organic metal parti- cles, Prog. Solid State Chem. 12 (1980) 185–271.

[51] C.F. Bohren, D.R. Huffman, Absorption and Scattering of Light by Small Particles, Wiley, New York, 1983.

[52] A. Henglein, Physicochemical properties of small metal particles in solution – mi- croelectronics reactions, chemisorptions, composite metal particles, and the atom- to-metal transition, J. Phys. Chem. 97 (1993) 5457–5471.

[53] P. Mulvaney, Surface plasmon spectroscopy of nanosized metal particles, Langmuir 12 (1996) 788–800.

[54] U. Kreibig, M. Vollmer, Optical Properties of Metal Clusters, Springer-Verlag, Berlin, 1995.

[55] U. Kreibig, U. Genzel, Optical-absorption of small metallic particles, Surf. Sci. 156 (1985) 678–700.

[56] W.C. Huang, J.T. Lue, Quantum-size effect on the optical-properties of small me- tallic particles, Phys. Rev. B 49 (1994) 17279–17285.

[57] M.M. Alvarez, J.T. Khoury, T.G. Schaaff, M.N. Shafigullin, I. Vezmer, R. Whetten, Optical absorption spectra of nanocrystal gold molecules, J. Phys. Chem. B 101 (1997) 3706–3712.

[58] Z. Liu, H. Li, X. Feng, S. Ren, H. Wang, Z. Liu, B. Lu, Formation effects and optical absorption of Ag nanocrystals embedded in single crystal SiO_2 by implantation, J. Appl. Phys. 84 (1998) 1913–1917.

[59] U. Kreibig, A. Althoff, H. Pressman, Veiling of optical single particle properties in many particle systems by effective medium and clustering effects, Surf. Sci. 106 (1981) 308–317.

[60] S. Dhara, Origin of shifts in the surface plasmon resonance frequencies for Au and Ag nanoparticles, in: C. Geddes (Ed.), Reviews in Plasmonics, 2016 Springer, Cham, 2015, pp. 275–294.

[61] Ph Buffat, J.P. Borel, Size effect on the melting temperature of gold particles, Phys. Rev. A 13 (1976) 2287–2298.

[62] T. Castro, R. Reifenberger, E. Choi, R.P. Andres, Size-dependent melting tempera- ture of individual nanometer-sized metallic clusters, Phys. Rev. B 42 (1990) 8548–8556.

[63] A. Miotello, G. De Marchi, G. Mattei, P. Mazzoldi, C. Sada, Clustering of gold atoms in ion-implanted silica after thermal annealing in different atmospheres, Phys. Rev. B 63 (2001) 075409.

[64] S.A. Gurevich, A.I. Ekimov, I.A. Kudrayavtsev, O.G. Lyublinskaya, A.V. Osinnskii, A.S. Usikov, N.N. Faleev, Growth of CdS nanocrystals in silicate-glasses and in thin SiO_2-films in the initial-stages of the phase-separation of a solid-solution, Semiconductors 28 (1994) 486–493.

[65] A.E. Hughes, S.C. Jain, Metal colloids in ionic crystals, Adv. Phys. 28 (1979) 717–828.

[66] G. De Marchi, G. Mattei, P. Mazzoldi, C. Sada, A. Miotello, Two stages in the kinetics of gold cluster growth in ion-implanted silica during isothermal annealing in oxidizing atmosphere, J. Appl. Phys. 92 (2002) 4249–4254.

[67] M. Mesnaoui, C. Parent, B. Tanguy, M. Maazaz, G. Le Flem, Spectroscopic properties of Ag^+ ions in phosphate-glasses of $NaPO_3$-$AgPO_3$ system, Eur. J. Solid State Inorg. Chem. 29 (1992) 1001–1013.

[68] L. König, I. Rabin, W. Schulze, G. Ertl, Chemiluminescence in the agglomeration of metal clusters, Science 274 (1996) 1353–1354.

[69] E. Borsella, E. Cattaruzza, G. De Marchi, F. Gonella, G. Mattei, P. Mazzoldi, A. Quaranta, G. Battaglin, R. Polloni, Synthesis of silver clusters in silica-based glasses for optoelectronics applications, J. Non-Cryst. Solids 245 (1999) 122–128.

[70] E. Borsella, G. Battaglin, M.A. Garcìa, F. Gonella, P. Mazzoldi, R. Polloni, A. Quaranta, Structural incorporation of silver in soda-lime glass by the ion-ex- change process: a photoluminescence spectroscopy study, Appl. Phys. A: Mater. Sci. Process. 71 (2000) 125–132.

[71] I. Belharouak, F. Weill, C. Parent, G. Le Flem, B. Moine, Silver particles in glasses of the 'Ag2-ZnO-P2O5' system, J. Non-Cryst. Solids 293 (2001) 649–656.

[72] L.A. Peyser, A.E. Vinson, A.P. Bartko, R.M. Dickson, Photoactivated fluorescence from individual silver nanoclusters, Science 291 (2001) 103–106.

[73] P. Gangopadhyay, R. Kesavamoorthy, S. Bera, P. Magudapathy, K.G.M. Nair, B.K. Panigrahi, S.V. Narasimhan, Optical absorption and photoluminescence spec- troscopy of the growth of silver nanoparticles, Phys. Rev. Lett. 94 (2005) 047403.

Table 1
List of the investigated samples, with relative label used in the text, and dose estimate for Er and Ag as from RBS analysis; the uncertainty is of the order of 10%.

Sample	Dose	
	Er/cm^2	Ag/cm^2
Er reference	6.8×10^{14}	–
Er+Ag as-impl.	6.4×10^{14}	6.1×10^{15}
Er+Ag 400 °C	6.6×10^{14}	6.1×10^{15}
Er+Ag 500 °C	6.7×10^{14}	5.8×10^{15}
Er+Ag 600 °C	6.3×10^{14}	5.6×10^{15}
Er+Ag 700 °C	6.6×10^{14}	4.7×10^{15}
Er+Ag 800 °C	6.4×10^{14}	3.9×10^{15}
Er+Ag 900 °C	7.0×10^{14}	2.7×10^{15}

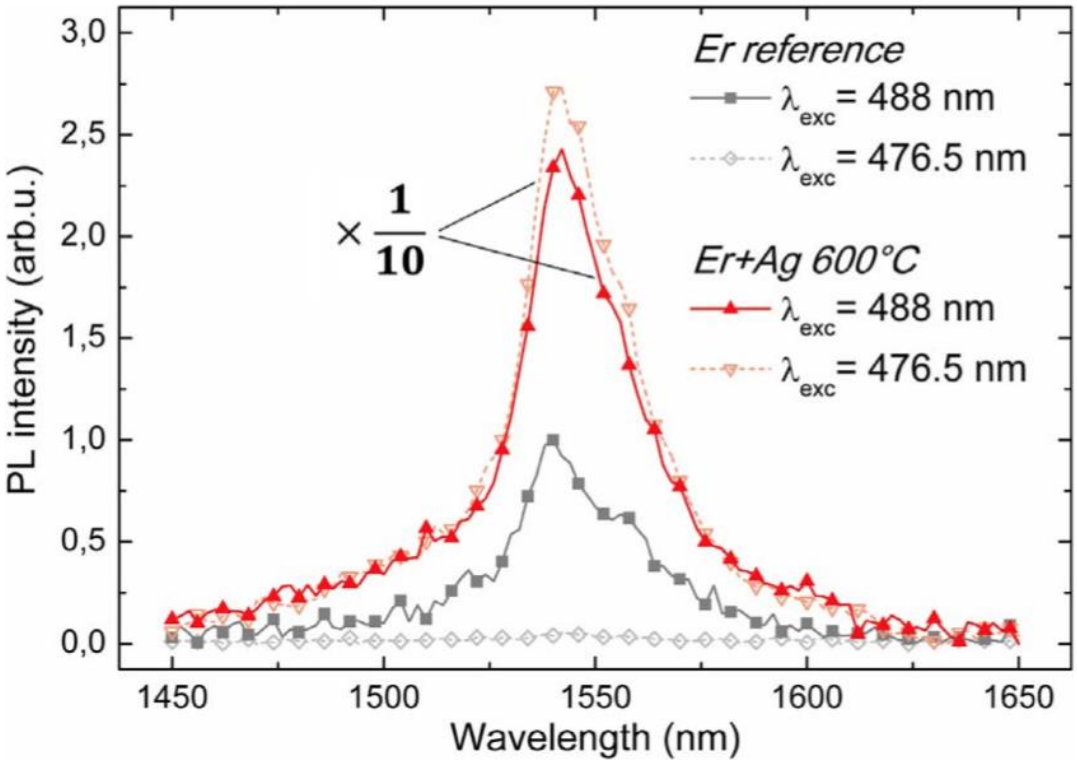

Fig. 1. In resonance (488 nm) and out of resonance (476.5 nm) Er PL emission in the 1450–1650 nm range for an Er-doped silica sample before and after Ag implantation followed by a 600 °C thermal treatment; PL intensity is normalized to 1 for the Er-doped reference, and accordingly re-scaled and divided by a factor of 10 for the co-implanted samples.

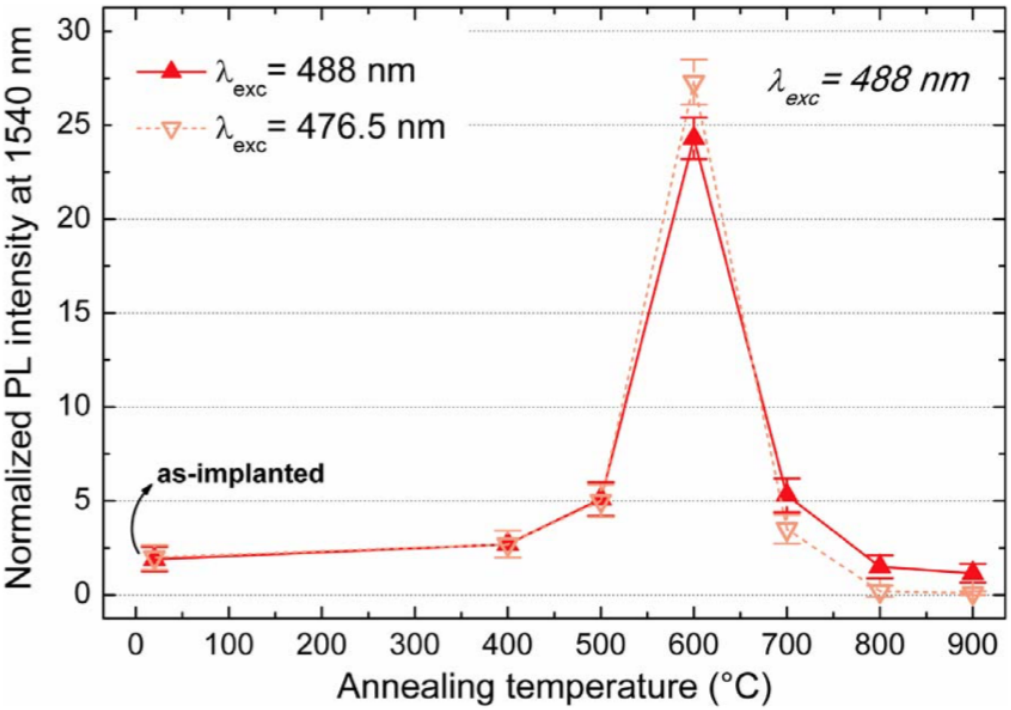

Fig. 2. Evolution of the 1.54 μm PL signal as a function of post-Ag implantation annealing temperature in both excitation conditions, with pumping power of 6.5 mW; the intensity values are normalized to the emission of the Er reference sample.

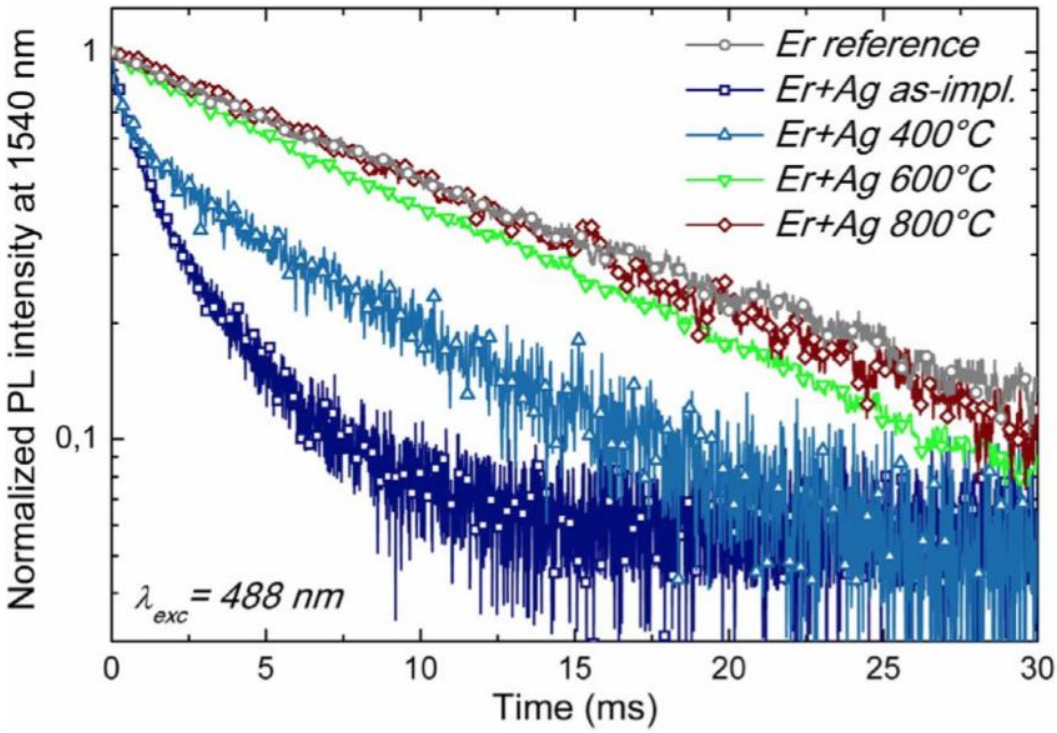

Fig. 3. Time decay curves of the 1.54 μm PL emission for the Er reference and Er and Ag co-doped samples annealed at different temperatures. Sample excitation was done by pumping with the 488 nm line of a 6.5 mW Ar laser, chopped at 9 Hz. Similar results were obtained under out-of-resonance excitation.

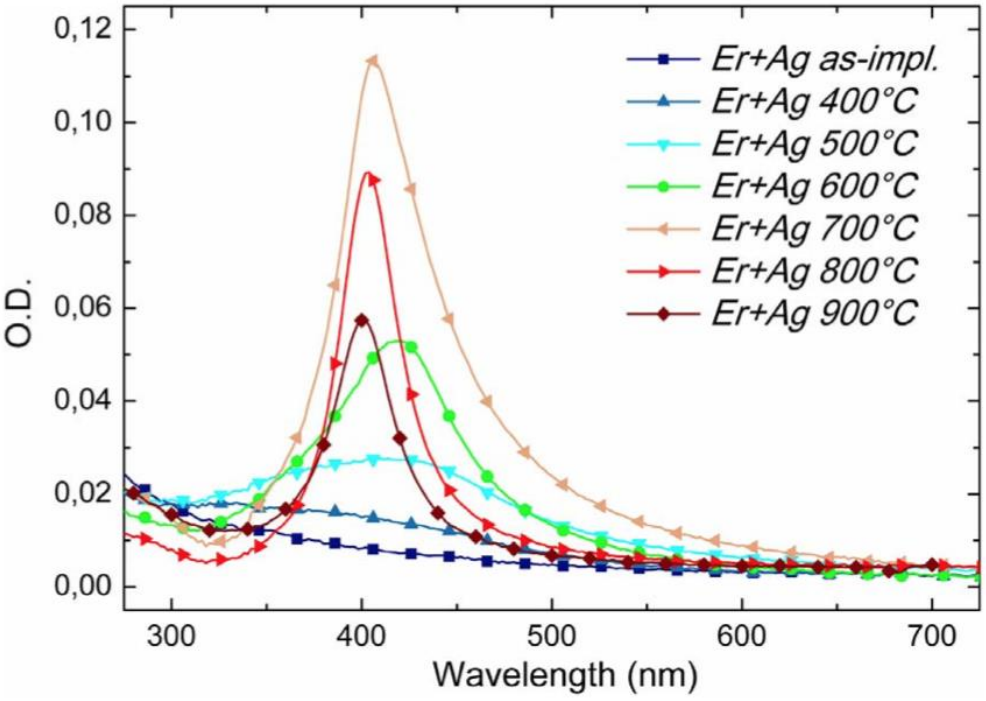

Fig. 4. Optical absorbance spectra of Er and Ag co-implanted samples annealed in N_2 atmosphere for 1 h at different temperatures.

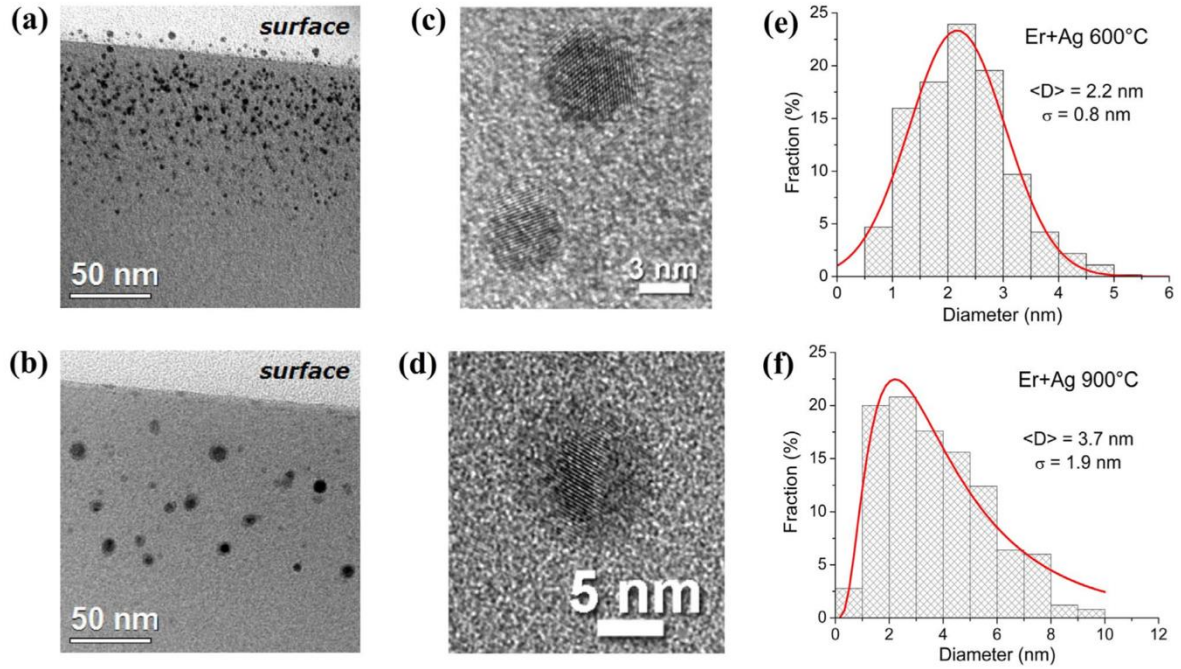

Fig. 5. (a,b) Cross-sectional bright-field and **(c,d)** high-resolution TEM images of Er and Ag co-doped samples annealed at 600 °C and 900 °C, respectively. **(e,f)** Histograms of the Ag cluster size distribution obtained from TEM analysis: average diameter < D > and standard deviation σ values from statistical analysis are reported.

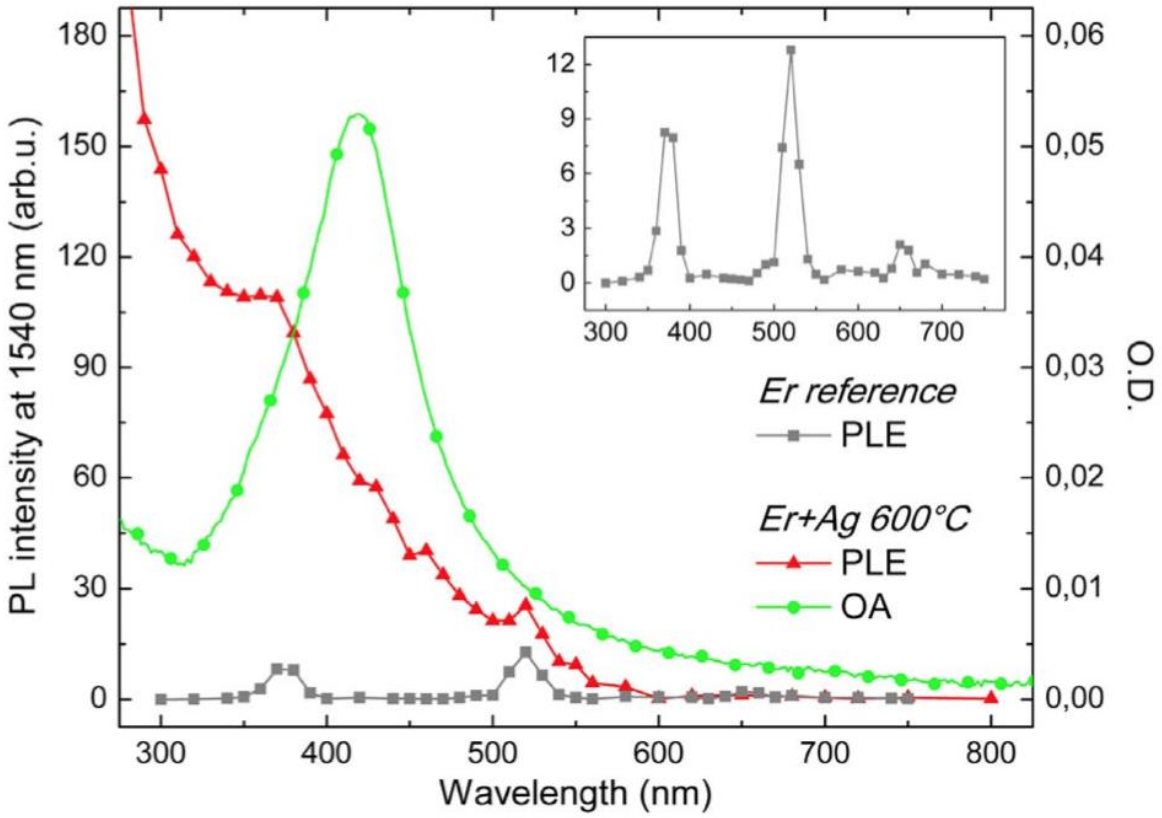

Fig. 6. Excitation spectra of the rare-earth emission at 1.54 μm for the Er reference sample (gray line) and the Er and Ag co-implanted sample annealed at 600 °C (red line); the intensity scale was calibrated by the PL measurements performed with the 488 nm Ar laser line. For comparison, the optical absorbance spectrum of the Er + Ag 600 °C sample (green line, intensity referred to the right scale) is reported. The Er reference excitation spectrum is zoomed in the inset. (For interpretation of the references to color in this figure legend, the reader is referred to the web version of this article.)